Gadolinium(III)-Loaded Nanoparticulate Zeolites as Potential High-Field MRI Contrast Agents: Relationship Between Structure and Relaxivity

Éva Csajbók,[a, b] István Bányai,[b] Luce Vander Elst,[c] Robert N. Muller,[c] Wuzong Zhou,[d] and Joop A. Peters*[a]

Dedicated to Professor Ernő Brücher on the occasion of his 70th birthday

Abstract: The effects of dealumination, pore size, and calcination on the efficiency (as expressed in the relaxivity) of Gd^{3+}-loaded zeolites for potential application as magnetic resonance imaging (MRI) contrast agents were studied. Partial dealumination of zeolites NaY or NaA by treatment with $(NH_4)_2SiF_6$ or diluted HCl resulted in materials that, upon loading with Gd^{3+}, had a much higher relaxivity than the corresponding non-dealuminated materials. Analysis of the ^1H NMR dispersion profiles of the various zeolites showed that this can be mainly ascribed to an increase of the amount of water inside the zeolite cavities as a result of the destruction of walls between cavities. However, the average residence time of water inside the Gd^{3+}-loaded cavities did not change significantly, which suggests that the windows of the Gd^{3+}-loaded cavities are not affected by the dealumination. Upon calcination, the Gd^{3+} ions moved to the small sodalite cavities and became less accessible for water, resulting in a decrease in relaxivity. The important role of diffusion for the relaxivity was demonstrated by a comparison of the relaxivity of Gd^{3+}-loaded zeolite NaY and NaA samples. NaA had much lower relaxivities due to the smaller pore sizes. The transversal relaxivities of the Gd^{3+}-doped zeolites are comparable in magnitude to the longitudinal ones at low magnetic fields (<60 MHz). However at higher fields, the transversal relaxivities steeply increased, whereas the longitudinal relaxivities decreased as field strength increased. Therefore, these materials have potential as T_1 MRI contrast agents at low field, and as T_2 agents at higher fields.

Keywords: contrast agents · gadolinium · lanthanides · magnetic resonance imaging · zeolites

Introduction

Magnetic resonance imaging (MRI) has been established as one of the most widely used diagnostic tools in clinical practice. Images with high spatial resolution, particularly of soft tissue, can be obtained with this technique. MRI images are generated from the NMR resonance of water protons, and the contrast depends essentially on three factors, 1) the water proton density, 2) the longitudinal relaxation time (T_1), and 3) the transversal relaxation time (T_2) of these protons. The contrast can be improved by shortening of the relaxation rates with the use of a paramagnetic contrast agent (CA), usually a Gd^{III} complex.[1,2] CAs currently on the market suffer from several disadvantages, the most important ones being poor efficiency in shortening of T_1 and T_2 and a lack of specificity. Once administered, these agents rapidly equilibrate nonspecifically between the intravascular and the interstitial compartments. For these reasons, a great deal of attention is dedicated to the development of new

[a] Dr. É. Csajbók, Dr. J. A. Peters
Laboratory of Applied Organic Chemistry and Catalysis
Delft University of Technology, Julianalaan 136
2628 BL Delft (The Netherlands)
Fax: (+31) 152-784-289
E-mail: j.a.peters@tnw.tudelft.nl

[b] Dr. É. Csajbók, Dr. I. Bányai
Department of Physical Chemistry
University of Debrecen
4010 Debrecen, Pf. 7 (Hungary)

[c] Prof. Dr. L. Vander Elst, Prof. Dr. R. N. Muller
Department of Organic and Biomedical Chemistry
NMR and Molecular Imaging Laboratory
University of Mons-Hainaut
7000 Mons (Belgium)

[d] Dr. W. Zhou
School of Chemistry
University of St Andrews
Haugh KY16 9ST, Fife (Scotland)

 DOI: 10.1002/chem.200500039

and more efficient contrast agents.[3,4] Delivery of higher doses of CA at the target site, by exploiting receptors or molecular determinants, would improve the visualization of abnormalities. A major problem encountered in imaging of receptors is their low concentration (typically 10^{-9}–10^{-13} mol g^{-1} of tissue) combined with the relative insensitivity of the technique.[5] Therefore, it is important that each targeting group is able to deliver a high payload of paramagnetic ions at a target. Several approaches have been used to achieve this, including Gd^{III} chelates loaded on high-molecular-weight carriers or into liposomes and conjugation of targeting vectors to iron oxide nanoparticles.[6]

Gadolite, a NaY zeolite in which Na^+ is partially exchanged for Gd^{3+}, has been developed by Balkus et al.[7,8] for the imaging of the gastrointestinal tract. Since each particle contains large amounts of Gd^{3+} ions, these systems are also of interest for the construction of targeting MRI contrast agents. Zeolites are chemically and thermally resistant crystalline aluminosilicates with a well-defined pore structure and channel system of molecular dimensions. The framework of zeolite Y is based on sodalite cages (which can be seen as a truncated octahedron) that are joined by oxygen bridges between the hexagonal faces.[9] Eight sodalite cages are linked, leaving a large central cavity or supercage with a diameter of 11.8 Å. The supercages share a twelve-membered ring with an open diameter of 7.4 Å. (Figure 1). Zeolite A is closely related to NaY in that its

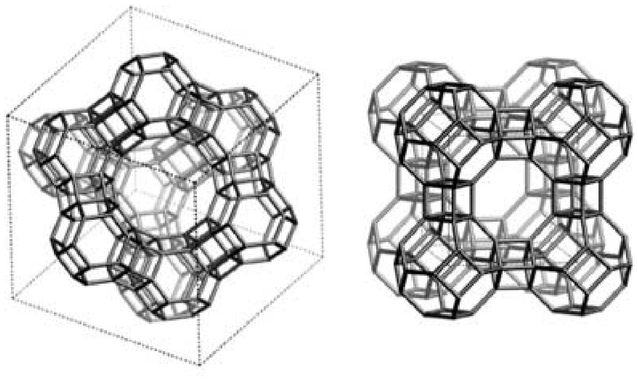

Figure 1. Structures of zeolite Y and zeolite A frameworks, viewed along the [111] and [001] planes, respectively. Reproduced with permission from the authors of reference [10].

framework is also made up of sodalite cages, but in a different rearrangement than in zeolite Y. Here, the eight sodalite cages are connected through the tetragonal faces, leading to a cubic arrangement. The supercage formed between the eight sodalite cages is somewhat smaller, with a diameter of 11.4 Å, whereas its eight-membered ring windows have an open diameter of only 4.1 Å (See Figure 1).

The monovalent cations balancing the negative charge of the AlO_4 units can be easily exchanged with trivalent cations; this allows incorporation of paramagnetic ions into the structure. Therefore, these aluminosilicate frameworks can serve as "carrier matrices" encapsulating Gd^{3+} ions. The electrostatic interaction between these trivalent cations and the negatively charged framework is strong and, consequently, leaching of the lanthanide ions is negligible.[8] Recently, we have presented a detailed study on the efficiency of Gd^{3+}-loaded NaY zeolite nanoparticles (80–100 nm) in relaxation-rate enhancement of water protons.[11] The efficiency expressed as the relaxivity (the relaxation-rate enhancement in s^{-1} by 1 mM Gd^{III}) ranged between 11.4 and 37.7 s^{-1} mM^{-1} at 60 MHz and 37 °C. The relaxivity increased drastically as the Gd^{3+}-loading decreased. The experimental data were explained by equations derived for a model considering a mechanism for the water exchange in two steps: first exchange between the water molecules in the coordination sphere of the zeolite-immobilized Gd^{3+} and the water in the interior of the zeolite pores, followed by the relatively slow diffusion of the water from the pores into the bulk water in a second step (see Figure 2).

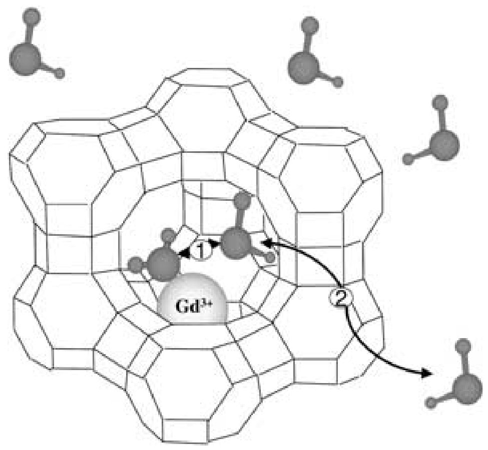

Figure 2. Schematic representation of the "two-step" model to account for the relaxivity in aqueous suspensions of Gd^{3+}-loaded zeolite Y.

The results of a simultaneous fitting of nuclear magnetic resonance dispersion (NMRD) and electron probe resonance (EPR) data showed that Gd^{3+} is efficiently immobilized and that the relaxivity is mainly limited by the relatively slow diffusion of water protons from the interior of the zeolite cavities towards the bulk water. The decrease of relaxivity observed with increased Gd^{3+} loading can be ascribed to the decrease in the number of water molecules inside the cavities.

Here, we present a study of the relationship between the longitudinal and transversal relaxivities of Gd^{3+}-exchanged zeolites and various parameters, including the pore size, the Si/Al ratio, and the location of Gd^{3+} ions within the cavities of the zeolite.

Results and Discussion

Dealumination: Dealumination of zeolites is a common method for the preparation of zeolites with a higher Si/Al molar ratio in the framework, making them more hydrophobic. Moreover, dealumination creates vacancies in the zeolite framework by removing some of the Al^{3+} ions; this may result in loss of crystallinity and an increase in pore size. Nanoparticles of zeolites NaY[11] and NaA[12] with average particle sizes of 80 and 130 nm, respectively, were dealuminated by using two different methods; a mild treatment and a more severe one. The mild dealumination was carried out with $(NH_4)_2SiF_6$. First, the Na^+ counterions were exchanged for NH_4^+ ions. At that stage, the zeolite frameworks were still fully intact as indicated by their XRD spectrum. Then treatment with $(NH_4)_2SiF_6$ resulted in a significant increase in the Si/Al ratio. XRD showed that this was accompanied by a loss in crystallinity (see Figure 3). As can be seen in Figure 3, the loss of crystallinity is larger for the relatively less stable zeolite A.

More severe dealumination was achieved by treatment of the zeolites with 0.5 M HCl. In this way, higher Si/Al ratios were obtained, but the loss in crystallinity was also higher; the XRD signals completely disappeared in the case of the zeolite A framework, indicating the collapse of the structure and the formation of amorphous material.

The various zeolites were loaded with Gd^{3+} by ion exchange with an aqueous solution of $GdCl_3 \cdot 6H_2O$ according to the procedure described previously.[11] The zeolites obtained were denoted as follows: for example, GdNaY-M-1.3, in which M or S indicates the method of dealumination (M = mild, S = severe, N = no dealumination), and the number gives the weight percent of Gd^{3+} in the zeolite concerned. High-resolution TEM (HR-TEM) images of the resulting zeolites confirmed the conclusions of the XRD measurements. Figure 4 shows, as an example, an HR-TEM image of a GdNaY-M-1.8 sample that displays some amorphous spherical particles accompanied by some particles with many point defects.

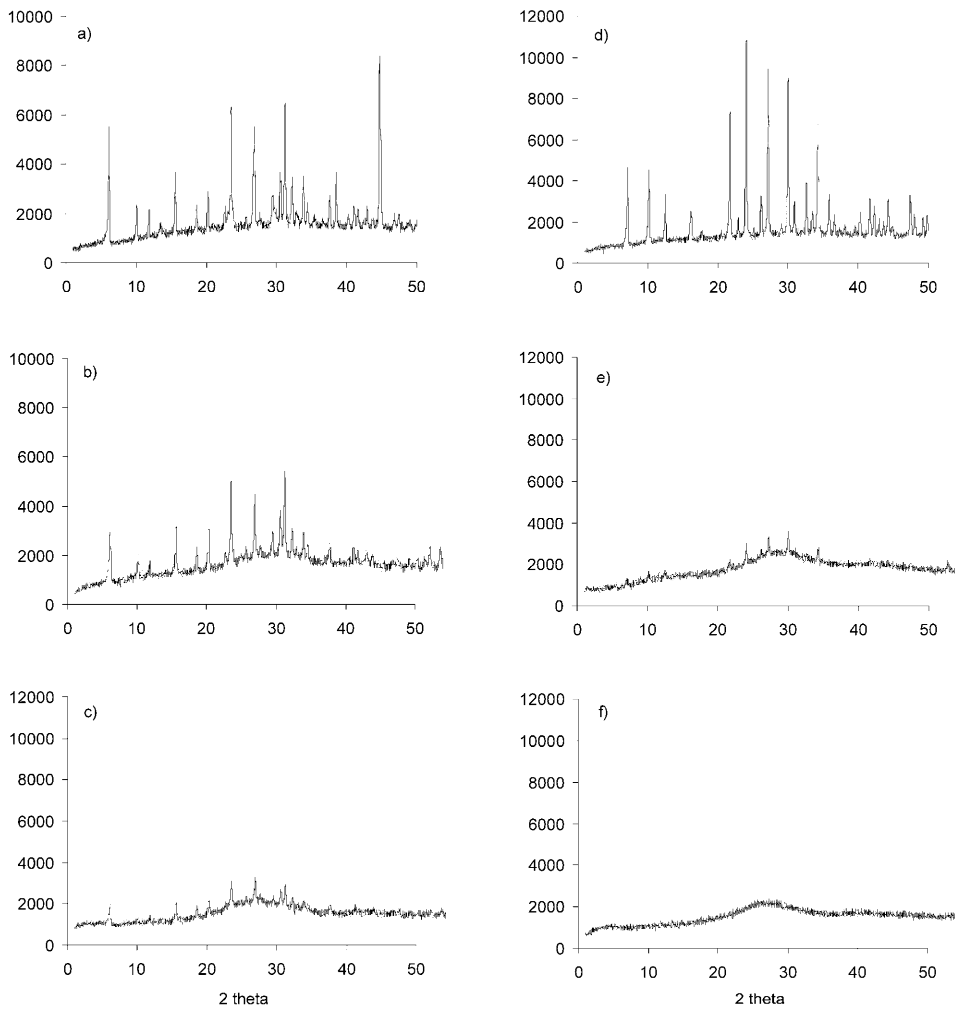

Figure 3. XRD patterns for zeolite NaY (left) and zeolite NaA (right); untreated (a,d), after dealumination with $(NH_4)_2SiF_6$ (b, e), after dealumination with HCl (0.5 M) (c, f).

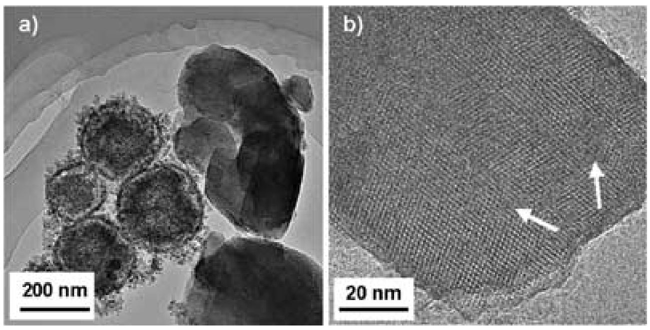

Figure 4. GdNaY-M-1.8 particles: a) TEM image and b) HR-TEM image. The arrows indicate point defects.

Effect of dealumination on r_1: To assess the efficacy of the various zeolites as MRI contrast agents and to evaluate the parameters governing the relaxivity, we measured the longitudinal relaxation rates of water protons in aqueous suspensions of these zeolites as a function of the Larmor frequency. The resulting NMRD profiles at 37 °C are displayed in Figure 5. For comparison, the previously studied non-dealuminated GdNaY zeolites with a similar Gd^{3+} content are in-

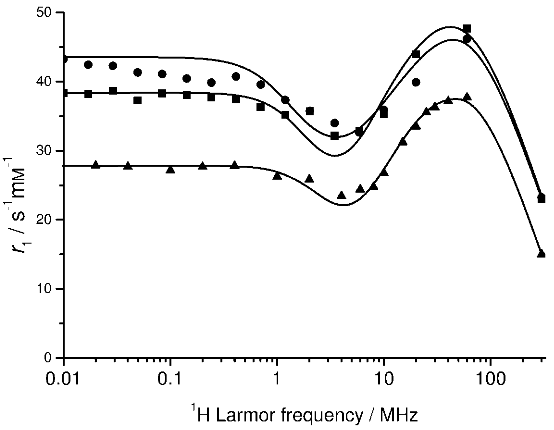

Figure 5. ^{1}H NMRD profiles of GdNaY-M-1.8 (squares) and GdNaY-S-2.3 (circles) with respect to that of GdNaY-N-1.3 (triangles)[11]. The curves are calculated with the best-fit parameters given in Table 1.

cluded in this figure. It can be seen that the relaxivity increases considerably upon dealumination, whereas the high local maximum between 50 and 100 MHz suggests that the mobility of the Gd^{3+} remains low.

Previously, we have shown that the longitudinal relaxivity of Gd^{3+}-loaded zeolites can be described well with a two-step mechanism (see above).[11] Equation (1) describes the relaxivity as a result of the exchange of the fast-relaxing water in the zeolite cavities and the bulk water outside the zeolite particles.

$$r_1 = \frac{1}{c_{Gd^{3+}}}\left(\frac{1}{T_{1,obs}} - \frac{1}{T_{1,dia}}\right) = \frac{x+q}{55500}\left(\frac{1}{T_{1,zeo}+\tau_{zeo}}\right) \tag{1}$$

Here, $c_{Gd^{3+}}$ is the Gd^{3+} concentration in mM, $T_{1,obs}$ is the measured longitudinal relaxation rate in the presence of the Gd^{3+}-exchanged zeolite, $T_{1,dia}$ is the measured longitudinal relaxation rate in the presence of the Gd^{3+}-free zeolite, x is the number of free water molecules inside the zeolite per Gd^{3+} ion (water molecules not coordinated to Gd^{3+}), q is the number of inner-sphere water molecules coordinating to the Gd^{3+} ion, τ_{zeo} is the residence time of the water protons inside the zeolite, and $T_{1,zeo}$ is the longitudinal relaxation time of free water protons inside the zeolite. The last parameter is given by Equation (2).

$$\frac{1}{T_{1,zeo}} = \frac{(q/x)}{\tau_m + T_{1m}[1+(q/x)]} \tag{2}$$

Here T_{1m} is the longitudinal relaxation rate of the Gd^{3+}-bound water molecules. This relaxation rate is dominated by the dipolar interaction and can be expressed by the Solomon–Bloembergen equation [see Eq. (3)].[13,14]

$$\frac{1}{T_{1m}} = \frac{2}{15}\left(\frac{\mu_0}{4\pi}\right)^2 \frac{\hbar^2\gamma_S^2\gamma_I^2}{r_{GdH}^6} S(S+1)\left(\frac{3\tau_{d1}}{1+\omega_I^2\tau_{d1}^2} + \frac{7\,\tau_{d2}}{1+\omega_S^2\tau_{d2}^2}\right) \tag{3}$$

Here, τ_m is the mean residence time of water protons in the inner sphere of the Gd^{3+} ions, r_{GdH} is the effective distance between the gadolinium electronic spin and the water protons, and γ_S and γ_I are the electron and proton gyromagnetic ratio, respectively. The correlation time τ_{di} is given by $\tau_{di}^{-1} = \tau_m^{-1} + \tau_R^{-1} + T_{ie}^{-1}$ ($i=1,2$). The rotational correlation time, τ_R, concerns the rotation of the Gd^{3+}/water proton vector. The electronic relaxation rates ($1/T_{ie}$) can be approximated by using Equations (4) and (5).[15,16]

$$\left(\frac{1}{T_{1e}}\right) = \frac{1}{25}\Delta^2\tau_\nu[4S(S+1)-3] \times \left(\frac{1}{1+\omega_S^2\tau_\nu^2} + \frac{4}{1+4\omega_S^2\tau_\nu^2}\right) \tag{4}$$

$$\left(\frac{1}{T_{2e}}\right) = \Delta^2\tau_\nu\left(\frac{5.26}{1+0.372\omega_S^2\tau_\nu^2} + \frac{7.18}{1+1.24\omega_S^2\tau_\nu^2}\right) \tag{5}$$

Here, ω_S is the Larmor frequency, Δ^2 is the trace of the square of the ZFS tensor, and τ_v is the correlation time for the modulation of ZFS.

The NMRD profiles obtained were fitted with Equations (1)–(5). The inner-sphere Gd^{3+}–H distance was fixed at 3.1 Å. We assumed that $q=7$ for Gd^{3+} ions inside the supercages of the hydrated zeolites. This is supported by extended X-ray absorption fine structure (EXAFS) investigations on Eu^{3+}-exchanged zeolite Y;[17] the results showed that one oxygen atom of the framework is coordinated to Eu^{3+}. A q value of 7 therefore results in an overall coordination number of 8 for Gd^{3+}. A good fit was obtained for the parameters given in Table 1; the calculated NMRD profiles are shown as the curves in Figure 5.

Table 1. Parameters obtained from fits of the NMRD profiles of the various Gd^{3+}-loaded zeolites at 37 °C.[a]

	GdNaY-S-2.3	GdNaY-M-1.8	GdNaY-N-1.3[b]	GdNaY-N-2.3[b]
dealumination method	HCl	$(NH_4)_2SiF_6$	none	none
Si/Al ratio	3.4	2.6	1.6	1.6
wt % Gd^{3+}	2.3	1.8	1.3	2.3
τ_R [ns]	>1	>1	>1	>1
τ_{zeo} [ms]	32(±0.4)	30(±0.5)	28	28
τ_m [ns]	1.6(±0.2)	1.6(±0.3)	3.6	5.6
τ_v [ps]	16(±1)	25(±1)	21	19
Δ^2 [10^{19} s^{-2}]	1.7(±0.5)	1.9(±0.6)	3.84	4.02
τ_{s0} [ps] [b]	316	173	103	71
x	94(±3)	90(±4)	60(±21)	37(±13)

[a] Standard deviations are given between parentheses. [b] Data from reference [11]. τ_{s0} is the low-field limiting value of the electronic relaxation time, calculated with the relation $\tau_{s0} = (12\Delta^2\tau_v)^{-1}$.

The NMRD profiles of the dealuminated zeolites could be fitted with any τ_R value larger than 1 ns. A similar phenomenon was previously observed with the non-dealuminated zeolites.[11] This demonstrates that the immobilization of Gd^{3+} in these zeolites is so effective that the region is reached in which the relaxivity becomes independent of τ_R.

A comparison of the dealuminated and non-dealuminated zeolite parameters shows that the main parameter responsible for the observed increase in r_1 upon dealumination is x, the number of uncoordinated water molecules in the interior of the zeolite per Gd^{3+} ion. This indicates that the dealumination has resulted in a substantial increase of the volumes of the cavities of the zeolite. Surprisingly, the values of the average residence times of water inside these zeolites (τ_{zeo}) only slightly increased (see Table 1). Most likely, increase of the pore size leads to leaching of Gd^{3+} during the purification of the Gd^{3+}-loaded zeolites by dialysis and, therefore, these destroyed cavities do not contribute to the relaxation enhancement. This is confirmed by the observation that it was impossible to load Gd^{3+} into severely dealuminated zeolite NaA. The slight increase in τ_{zeo} is possibly due to the blocking of some of the cavity windows in the dealuminated NaY zeolites, although it is debatable as to whether the difference in τ_{zeo} is significant.

The increase in x upon dealumination is accompanied by a decrease in τ_m, which means that the exchange between the water molecules coordinated to the Gd^{3+} ions and the water in the zeolite cavities becomes faster. When the x value increases, there will be more non-coordinated water molecules per Gd^{3+} ion inside the cavities; this makes the probability of a water molecule being located in the inner coordination sphere of Gd^{3+} lower and, therefore, τ_m decreases. A similar phenomenon was observed upon a decrease of the Gd^{3+} loading in the non-dealuminated zeolites.[11]

The electronic relaxation times increased upon dealumination (see Table 1). This suggests that an interaction between neighboring Gd^{3+} ions is less than in the non-dealuminated samples. In larger cavities the probability of two Gd^{3+} ions being in close proximity may be larger than in small cavities, and this could produce a significant electronic relaxation effect, as previously demonstrated with dimeric Gd^{3+} chelates.[18] A similar effect was also observed upon increase of the Gd^{3+}-loading in the non-dealuminated zeolite NaY.[11]

Effect of pore size on r_1: To investigate the effect of pore sizes on the relaxivities, we studied Gd^{3+}-exchanged zeolite A. This zeolite has supercages of about the same size as zeolite NaY (11.4 Å, see above), but here the access to these cages is through an eight-membered ring with a diameter of only 4.1 Å as compared to 7.4 Å for zeolite NaY. The longitudinal water proton relaxation rates in suspensions were much smaller than in suspensions of GdNaY. Unfortunately, they were too low to allow recording of NMRD profiles at Larmor frequencies below 20 MHz with the use of a fast-field-cycling NMR spectrometer. However, we measured the relaxivities with fixed-field spectrometers at 20, 60, and 300 MHz. The results (see Figure 6) show the dramatic effect that the pore sizes and, therefore, the diffusion rates have on the relaxivity. Simulations of the relaxivity by using Equations (2)–(5) indicate that τ_{zeo} is about 190 ns in this case, if it is assumed that all other parameters are the same as in GdNaY-N-1.3. Under the same conditions, the value of τ_{zeo} of the latter zeolite is only 28 ns.

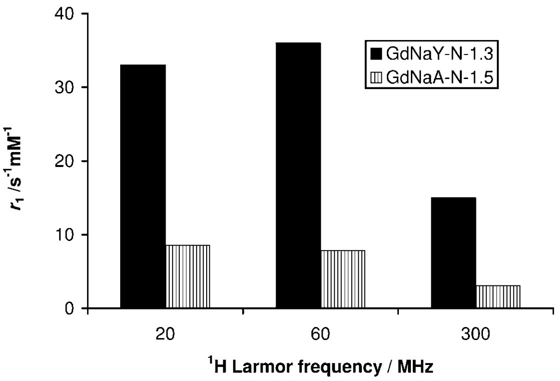

Figure 6. r_1 relaxivities of GdNaY-N-1.3, Si/Al = 1.6[11], and GdNaA-N-1.5, Si/Al = 1.0 samples at 37 °C and at different fields.

The dealuminated GdNaA samples behaved similarly to the dealuminated GdNaY samples; "mild dealumination" with $(NH_4)SiF_6$ resulted in a relatively high relaxivity with respect to the comparable non-dealuminated zeolite, but it still had a lower relaxivity than the Gd^{3+}-loaded dealuminated NaY zeolites. However, the "severe dealumination" with 0.5 M HCl completely destroyed the framework; the zeolite could not even retain immobilized Gd^{3+}. This was reflected in a very low Gd^{3+} content and a very low relaxivity for these samples.

The relaxivities of the non-dealuminated and mildly dealuminated GdNaA samples increased with increasing temperature (Figure 7); this is in agreement with limitation of the proton relaxivity by the relatively slow water diffusion.

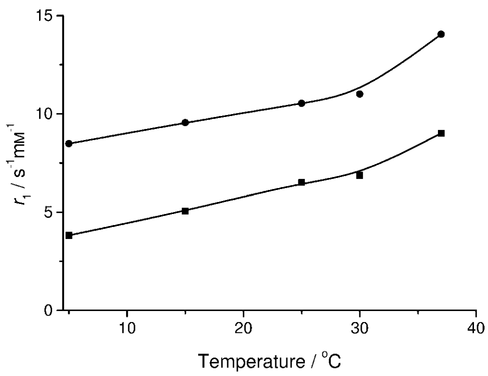

Figure 7. Temperature dependence of r_1 relaxivities of GdNaA-N-1.5 (Si/Al = 1.0) (squares) and GdNaA-M-1.7 (Si/Al = 1.7) (circles) at 20 MHz. The curves are guides to ease data visualization.

The dramatic effect of the pore size on the r_1 relaxivity is in line with the recently reported high relaxivity of a mesoporous material in which Gd^{3+} was incorporated.[19] Since this material had a pore size of 2 nm,[19] it may be expected that the diffusion no longer limits the relaxivity. Unfortunately, no full NMRD profile was reported, but the longitudinal relaxivity at 400 MHz and 23 °C was 23.6 s^{-1} mM^{-1} for a material in which 1.6 % Gd was incorporated.

Effect of calcination on r_1: It has been shown by luminescence[20] and MAS NMR spectroscopy[21] that lanthanide ions in Ln^{3+}-exchanged zeolite NaY move irreversibly from the supercages into the the sodalite cages or its hexagonal entrance window upon heat treatment at temperatures of 200 °C. The water-exchange rate between the sodalite cages and the supercages (1 mol in 4 days at room temperature)[22] or between the sodalite cages and the bulk water is very low, so we can consider these lanthanide ions to be "lost", since they do not contribute to the relaxivity enhancement effect. However, Gd^{3+} ions in the hexagonal windows of the sodalite cages may still be in contact with the water of the supercages. On the other hand, x is expected to increase upon calcination and would give rise to a positive contribution of the relaxivity. Therefore we studied the effect of the calcination at various temperatures on the room-temperature r_1 and r_2 relaxivities (300 MHz) of the GdNaY-N-1.3 sample.

The sample calcined up to 300 °C did not show a significant change in relaxivity relative to the starting material. However, the samples calcined at 400 and 500 °C had relaxivities reduced by more than 50 % relative to the untreated GdNaY sample (Figure 8). It is unlikely that all Gd^{3+} ions

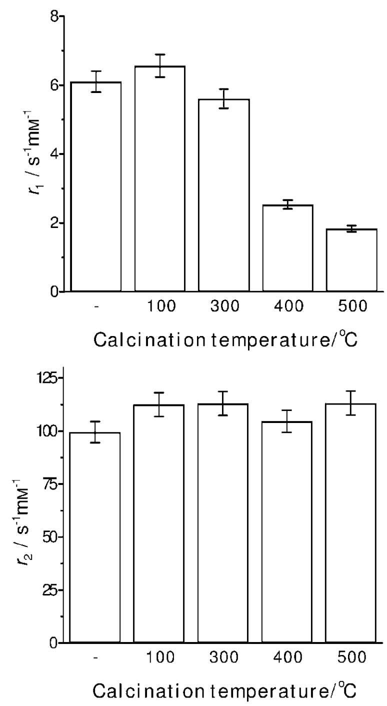

Figure 8. Effect of calcination of GdNaY-N-1.3 on its relaxivities r_1 (top) and r_2 (bottom) at 300 MHz and 25 °C.

of the zeolite calcined at temperatures higher than 300 °C are located inside the sodalite cages. More likely, the Gd^{3+} ions are located in the hexagonal windows of the sodalite cages. In these windows they will be coordinated by the three oxygen atoms. Only the water molecules that can be coordinated on the side of the supercages play a role in the relaxivity. Sterically, there will be space for coordination of a maximum of two water molecules from that side. A reduction of q from 7, for the uncalcined sample, to 2, after heating, is in agreement with the reduction of relaxivity observed.

Transversal relaxation rates: The transversal relaxivities (r_2) of the zeolite samples were of the same order of magnitude as r_1 up to about 10 MHz, but upon further increase of the magnetic field, the value of r_2 increased steeply, while r_1 decreased (see Figure 9). Interestingly, the r_2 relaxivities at

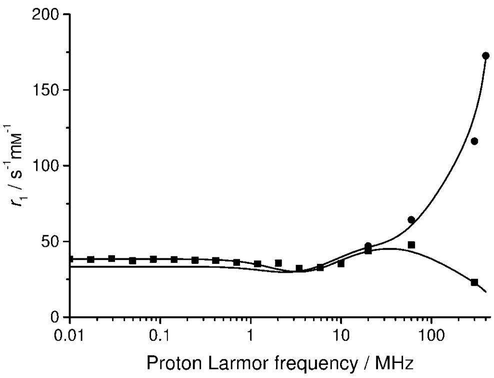

Figure 9. Longitudinal and transversal NMRD profiles ($i = 1,2$) at 37 °C for GdNaY-M-1.8: r_1 (squares), r_2 (circles). The curves are calculated with the equations described in the text.

300 MHz of the calcined GdNaY-N-1.3 samples are the same as those of the uncalcined sample (see Figure 8), whereas the r_1 relaxivity decreased significantly upon calcination due to the movement of the Gd^{3+} ion from the supercage to the sodalite cage. This suggests that the propagation of r_2 by means of a two-step mechanism plays a minor role. For this mechanism the r2 relaxivity can be derived by Equations (6)–(8) (see also the Appendix).

$$r_2 = \frac{1}{1000}\frac{(x+q)}{55.5\tau_{zeo}}\frac{\frac{1}{T_{2,zeo}}\left(\frac{1}{T_{2,zeo}}+\frac{1}{\tau_{zeo}}\right)+\Delta\omega_{zeo}^2}{\left(\frac{1}{T_{2,zeo}}+\frac{1}{\tau_{zeo}}\right)^2+\Delta\omega_{zeo}^2} \quad (6)$$

$$\frac{1}{T_{2,zeo}} = \frac{q}{(x+q)T_{2m}} \quad (7)$$

$$\frac{1}{T_{2m}} = \frac{1}{15}\left(\frac{\gamma_I^2 g^2 \mu_B^2}{r_{GdH}^6}\right)S(S+1)\left(\frac{\mu_0}{4\pi}\right)^2\left(13\frac{\tau_{d2}}{1+\omega_S^2\tau_{d2}^2}+3\frac{\tau_{d1}}{1+\omega_I^2\tau_{d1}^2}+4\tau_{d1}\right) \quad (8)$$

Here, $\Delta\omega_{zeo}$ is the difference in resonance frequency between the water in the zeolite cavities and the bulk water,

$T_{2,zeo}$ is the ^{1}H transversal relaxation time of water inside the zeolite cavity and T_{2m} is that of the Gd^{3+}-bound water molecules. The latter relaxation time can be described by Equation (8). The contribution of the Curie mechanism to $1/T_2$ is negligible for Gd^{3+}; even considering that the τ_R values are very large in this case, this contribution at 300 MHz is still an order of magnitude smaller than that of the dipolar contribution. Simulations of r_2 profiles using Equations (6)–(8), and the best-fit parameters of the r_1 NMRD curve for GdNaY-M-1.8 showed that the low-field part (<100 MHz) of the r_2 profile could be well explained with this mechanism. However, the maximum r_2 possible with this model is around $60\,s^{-1}mM^{-1}$, while the measured r_2 at 400 MHz is $173\,s^{-1}mM^{-1}$. Therefore, it can be concluded that an additional transversal relaxation-rate enhancement mechanism is operative at high fields. Most likely, the strong field-dependent transversal relaxation-rate enhancement can be rationalized by a dephasing due to the diffusion of water protons along the weakly magnetized zeolite particles. Brooks has shown that this T_2-shortening can be well reproduced by a chemical-exchange model. In the long echo limit the relaxation enhancement can be given by Equation (9).[23]

$$\frac{1}{T_{2,CE}} = F_a F_b \tau_{ex} (\Delta\omega)^2 \tag{9}$$

Here F_a and F_b are the fractions of protons at each site, namely, in a shell around the particles and in the bulk, respectively. The parameter τ_{ex} is related to the residence times of the protons at the two sites concerned through: $\tau_{ex}^{-1} = \tau_a^{-1} + \tau_b^{-1}$. After taking into account this additional contribution, the experimental r_2 profile was reproduced with the parameters obtained from the fitting of the r_1 profile and with $F_aF_b\tau_{ex} = 7.9\times10^{-10}$ s and $\Delta\delta = 151$ ppm. Here, $\Delta\delta$ is the difference in chemical shift between the zeolite surface and the bulk water (see Figure 9).

Conclusion

The results in this paper show that the supercages of zeolite NaY can be enlarged by partial destruction of the framework. Upon loading with Gd^{3+}, these dealuminated zeolites are significantly more efficient in increasing the longitudinal rates of water protons than the non-dealuminated analogues. The longitudinal relaxation-rate enhancement can be ascribed to a two-step model, based on the assumption that the interior of the zeolites contains a concentrated aqueous solution of Gd^{3+} that exchanges with the bulk water outside the zeolite. The increase in longitudinal relaxivity upon dealumination can be attributed to the larger number of water molecules inside the zeolite that experience the paramagnetic relaxation-rate enhancement. The diffusion rate between the cavities and the bulk does not change significantly upon dealumination, which suggests that the windows giving access to Gd^{3+}-loaded cavities are intact. The importance of diffusion is, however, demonstrated by the dramatic decrease in relaxivity going from GdNaY to GdNaA, which has significantly smaller pores. For GdNaY, a maximal r_1 is reached at about 60 MHz. Under these conditions, the value of the transversal relaxivity r_2 is about equal to that of r_1, but at higher magnetic fields r_2 becomes much larger than r_1.

Experimental Section

Materials: The batch of zeolite NaY used in this study was a gift from Akzo Nobel. The chemicals used for the synthesis of zeolite NaA (aluminum isopropoxide, tetramethylammonium hydroxide, Ludox HS30 and NaOH), $GdCl_3 \cdot 6H_2O$, $DyCl_3 \cdot 6H_2O$ and xanthan gum were purchased from Aldrich.

Zeolite NaA: The zeolite NaA nanoparticles were prepared according to the literature method of Traa et al.[12] A mixture of tetramethylammonium hydroxide (80.4 g), an aqueous NaOH solution (4.8 g, 1 M), aluminum isopropoxide (6.0 g) and distilled water (15.6 g) was stirred in a 250 mL Nalgene polypropylene bottle until all aluminum isoproproxide was dissolved. In another polypropylene bottle, water (16.0 g) and Ludox HS30 (18 g) were mixed. This mixture was added to the basic aluminum isoproproxide solution, and the polypropylene bottle was capped tightly. The opaque solution obtained was slowly stirred magnetically at 80 °C in an oil bath for 24 h. After 2 h, the solution became clear; the final product was a white solid dispersed in the mother liquor. The bottle was cooled by an ice/water mixture, and the zeolite was separated by centrifugation at 4000 rpm for 60 min at 5 °C. The resulting solid was washed three times with the appropriate amount of water under ultrasonication, followed by centrifugation at 4000 rpm for 60 min at room temperature. The NaA zeolite was dried at 80 °C overnight and then calcined using the following temperature ladder: 25 °C→5 °C min^{-1}→150 °C, 1 h→5 °C min^{-1}→550 °C, 3 days→−5 °C min^{-1}→25 °C. The weight of the resulting NaA sample was 1.0 g.

Dealuminations: Dealumination of both NaA and NaY was conducted by using two different procedures: 1) mild dealumination using $(NH_4)_2SiF_6$ (Riedel-de Haën) and 2) a severe method with HCl (0.5 M). In the mild procedure, highly ammonium-exchanged zeolite was made by subjecting the zeolite (1 g) to ion-exchange with NH_4NO_3 solution (20 mL, 1 M, Merck) at 60 °C for 1 h. After recovery of the product and washing, the zeolite samples were dried at room temperature to avoid damage to the zeolite structure. For the actual mild dealumination step, the samples of the NH_4-exchanged zeolites were dispersed by ultrasonic treatment in ammonium acetate solution (70 mL, 1 M, Aldrich) in 125 mL polypropylene Nalgene flasks. Then, $(NH_4)_2SiF_6$ (0.05–0.25 g) was added with vigorous stirring. The flasks were capped and were kept at 60 °C for 1 h in an oil bath under continued vigorous stirring. The solids were separated by centrifugation and washed three times with demineralized water to remove all soluble byproducts. For stabilization, the obtained materials were treated twice with sodium acetate solution (50 mL, 1 M, Aldrich) and then washed again with water (50 mL) three times. The solid samples were dried at room temperature.

The severe dealumination of NaA and NaY was achieved by stirring NaA (0.6 g) or NaY (0.5 g) with HCl (10 mL, 0.5 M) at 80 °C for 4 h. The solid obtained was separated by centrifugation and washed three times with demineralized water (10 mL) to remove all soluble byproducts. The solid was dried at room temperature.

Gd^{3+} exchange of the zeolites: Prior to Gd^{3+} exchange, the four dealuminated NaA and NaY samples were stirred with NaCl (10 mL, 1 M) overnight. The Gd^{3+} exchange was performed with NaA (0.3 g, dealuminated by HCl), NaA (0.5 g, dealuminated by $(NH_4)_2SiF_6$), NaY (0.2 g, dealuminated by HCl), and NaY (0.3 g, dealuminated by $(NH_4)_2SiF_6$). The solid samples were dispersed under ultrasonication in demineralized water (2–3 mL). The pH values of the samples were 4.1, 8.4, 7.3, and 6.8, respectively. The pH was adjusted to 5.5 with HCl (0.1 M) or NaOH (0.1 M) and $GdCl_3 \cdot 6H_2O$ (13–19 mg) was then added. The samples were stirred overnight, after which the Gd^{3+}-exchanged zeolites were subjected to dialysis against water for 24 h (using a Sigma-Aldrich dialysis tube, 1 cm diameter, 12 KD cut-off). The water was removed by rotational evaporation, and the Gd^{3+}-exchanged zeolites were dried at room temperature.

Calcination: Samples of GdNaY (1.3 wt % Gd) described previously[11] were heated in a calcination oven with a continuous, mild air flow for 1 h at 100, 300, 400, or 500 °C. The temperature was raised to the desired temperature at a rate of 5 °C min^{-1} . Then after heating for 1 h, the sample was cooled down at a rate of 5 °C min^{-1}.

Methods: All zeolites used were characterized by XRD, ^{29}Si and ^{27}Al MAS NMR spectroscopy, and ICP (ICP = inductively coupled plasma). The XRD patterns were obtained with a D-5000 Siemens diffractometer, with Ni-filtered $Cu_{K\alpha}$ radiation ($\lambda = 1.5406$ Å). MAS NMR spectra were recorded on a Varian VXR-400 S spectrometer with resonance frequencies of 79.460 MHz (^{29}Si) and 104.229 MHz (^{27}Al). High-resolution transmission electron microscopy (HRTEM) was performed on a Jeol JEM-2010 electron microscope operated at 200 kV. The NMRD measurements were performed on a Stelar apparatus, the T_1 and T_2 measurements at 20 and 60 MHz were performed on Bruker Minispec relaxometers. Those at 300 and 400 MHz were measured on a Varian Inova-300 and a Varian VXR-400 S spectrometer, respectively. The T_1 measurements were made with an inversion–recovery sequence and the T_2 measurements with a Carr–Purcell spin-echo sequence with two refocusing pulses for which the echo interval was varied.

For the NMRD measurements, the Gd^{3+}-exchanged zeolite under study (10 mg) was dispersed under ultrasonication in demineralized water (10 cm^3), containing xanthan gum (0.2 %) as surfactant. The diamagnetic term was measured by using NaY or NaA (10 mg) dispersed in demineralized water (10 cm^3), containing xanthan gum (0.2 %) as surfactant.

Appendix

Derivation of Equations (6) and (7): The two-step model described previously for the field-dependence of r_1 in aqueous suspensions of Gd^{3+}-loaded zeolites can also be applied for the r_2 values. For both steps of this model, we can derive approximate equations from the exact solutions of the Bloch equations for the transverse relaxation time of a system in which water protons undergo chemical exchange between two magnetically distinct environments A and B [Eq. (10)].[24–26]

$$\frac{1}{T_2} = -A_2 \pm \left\{ \frac{G + (G^2 + H^2)^{1/2}}{2} \right\} 1/2 \tag{10}$$

Here G, H, and A_2 are given by Equations (11)–(13).

$$G = \frac{\left(\frac{1}{\tau_{2A}} - \frac{1}{\tau_{2B}}\right)^2}{4} + \frac{1}{\tau_a \tau_b} - \frac{(\Delta\omega_A - \Delta\omega_B)^2}{4} \tag{11}$$

$$H = \frac{\left(\frac{1}{\tau_{2A}} - \frac{1}{\tau_{2B}}\right)(\Delta\omega_A - \Delta\omega_B)}{2} \tag{12}$$

$$A_2 = \frac{1}{2}\left(\frac{1}{\tau_{2A}} + \frac{1}{\tau_{2B}}\right) \qquad \frac{1}{\tau_{2A}} = \frac{1}{T_{2A}} + \frac{1}{\tau_a} \tag{13}$$

T_{2A} is the intrinsic relaxation time in the A environment and τ_a is the corresponding residence time. Analogous definitions apply for the B environment. $\Delta\omega_A$ and $\Delta\omega_B$ are the frequencies of the protons in the A and B environments, respectively. Considering the B system to represent the water inside the zeolite cavities and the A system to represent the bulk water, we can assume that $T_{1A} \gg T_{1B}$ and $\tau_a \gg \tau_b$. If we take $\Delta\omega_A = 0$ (on resonance), we obtain Equation (14) and, consequently, r_2 is given by Equation (6) shown previously in the main text.

$$\frac{1}{T_2} = \frac{\left[\left(\frac{1}{\tau_{2A}\tau_{2B}} - \frac{1}{\tau_a \tau_b}\right)/\tau_{2B}\right] + \frac{\Delta\omega_B}{\tau_{2A}}}{\frac{1}{\tau_{2B}^2} + \Delta\omega_B^2} \tag{14}$$

The inequality $\tau_a \gg \tau_b$ does not hold for the interior of the zeolite. Therefore, to evaluate $T_{2,zeo}$, we assume a chemical exchange between two magnetically distinct environments in a concentrated system; water protons in the interior of the zeolite (A environment) and water molecules coordinated to the Gd^{3+} ion (B environment). In fast exchange, for which the conditions are $(1/\tau_a + 1/\tau_b) \gg |(1/T_{2A}) - (1/T_{2B})|$ and $1/\tau_{ab} \gg (\Delta\omega_A - \Delta\omega_B)$, the transverse relaxation time is given by Equation (15), in which f_a and f_b are the mole fractions and τ_{ab} is given by $1/\tau_{ab} = 1/\tau_a + 1/\tau_b$.

$$\frac{1}{T_2} = \frac{f_a}{T_{2A}} + \frac{f_b}{T_{2B}} + f_a f_b \tau_{ab} (\Delta\omega_A - \Delta\omega_B)^2 \tag{15}$$

If we take $\Delta\omega_A = 0$ and then substitute the parameters used for the two-site system in the zeolite cavities we obtain Equation (16), describing $1/T_{2,zeo}$.

$$\frac{1}{T_{2,zeo}} = \frac{x}{(x+q)T_{2,water}} + \frac{q}{(x+q)T_{2m}} + \frac{xq}{(x+q)}\tau_m (\Delta\omega_m)^2 \tag{16}$$

Here, T_{2m} is the transverse relaxation time of inner-sphere water protons, $T_{2,water}$ is the transverse relaxation time of water protons not coordinated to Gd^{3+} inside the zeolite cavities, and $\Delta\omega_m$ is the chemical shift difference induced by the Gd^{3+} ions. The other parameters have the same meaning as above.

Assuming that T_{2m} is governed by the dipole–dipole interactions, then T_{2m} is described by Equation (8) (see main text above). Since the parameters determining T_{2m} are the same as those for T_{1m}, we performed a simulation to estimate the field-dependence of T_{2m} with respect to T_{1m}. For this calculation we used the parameters obtained from the fitting of the r_1 NMRD profile for the GdNaY/F-1.8 sample. We found that at lower fields T_{1m} and T_{2m} are equal, while, because of the $4\tau_{d1}$ term, at higher fields (> 0.1 T) T_{2m} gradually becomes shorter than T_{1m} and above 1 T the difference becomes significant. From the simulation, the value of T_{2m} was estimated to be less than 3×10^{-6} s over the whole range of magnetic fields studied. Therefore, the first term of Equation (16) is negligible with respect to the second term, containing *$1/T_{2m}$*. Furthermore, the simulations show that the third term of Equation (16) is negligible as well. Consequently, this equation can be simplified to Equation (7) given in the main text above.

Acknowledgements

This research was carried out within the framework of the European-funded EMIL program (LSHC-2004–503569) and of EU COST action D18: “Lanthanide chemistry for diagnosis and therapy”. Thanks are due to the EU for financial support via a Marie Curie training site-host fellowship (QLK5-CT-2000–60062). We are grateful to Prof. J. C. Jansen for helpful discussions and to Giovannia A. Pereira for assistance in performing some NMR experiments. Two of the authors (I.B. and É.C.) thank the the Hungarian National Science Research Foundation for financial support (OTKA T035127). L.V.E and R.N.M thank the ARC Program 00/05–258 of the French Community of Belgium.

[1] *The Chemistry of Contrast Agents in Medical Magnetic Resonance Imaging* (Eds.: A. E. Merbach, É. Tóth), Wiley, Chichester, **2001**.

[2] P. Caravan, J. J. Ellison, T. J. McMurry, R. B. Lauffer, *Chem. Rev.* **1999**, *99*, 2293.

[3] L. Frullano, J. Rohovec, J. A. Peters, C. F. G. C. Geraldes, *Top. Curr. Chem.* **2002**, *221*, 25.

[4] V. Jacques, J. F. Desreux, *Top. Curr. Chem.* **2002**, *221*, 123.

[5] A. D. Nunn, K. E. Linder, M. F. Tweedle, *Q. J. Nucl. Med.* **1997**, *41*, 155.

[6] R. N. Muller, L. Vander Elst, A. Roch, J. A. Peters, É. Csajbók, P. Gillis, Y. Gossuin, *Adv. Inorg. Chem.* **2005**, *57*, 239.

[7] K. J. Balkus Jr., A. D. Sherry, S. W. Young, *US Patent* 5122363 A, **1992**.

[8] I. Bresinska, K. J. Balkus Jr., *J. Phys. Chem.* **1994**, *98*, 12989.

[9] H. van Bekkum, P. A. Jacobs, E. M. Flanigen, J. C. Jansen, *Introduction to Zeolite Science and Practice*, 2nd ed., Elsevier, Amsterdam, **2001**.

[10] C. Baerlocher, W. M. Meier, D. H. Olson, *Atlas of Zeolite Framework Types*, 5th ed., Elsevier, Amsterdam, **2001**.

[11] C. Platas-Iglesias, L. Vander Elst, W. Zhou, R. N. Muller, C. F. G. C. Geraldes, T. Maschmeyer, J. A. Peters, *Chem. Eur. J.* **2002**, *8*, 5121.

[12] R. A. Rakoczy, Y. Traa, *Microporous Mesoporous Mater.* **2003**, *60*, 69.

[13] I. Solomon, *Phys. Rev.* **1955**, *99*, 559.

[14] N. Bloembergen, L. O. Morgan, *J. Chem. Phys.* **1961**, *34*, 842.

[15] D. H. Powell, A. E. Merbach, G. González, E. Brücher, K. Micskei, M. F. Ottaviani, K. Köhler, A. Von Zelewsky, O. Ya. Grinberg, Ya. S. Lebedev, *Helv. Chim. Acta* **1993**, *76*, 2129.

[16] A. D. McLachlan, *Proc. R. Soc. London Ser. A* **1964**, *280*, 271.

[17] F. J. Berry, M. Carbucicchio, A. Chiari, C. Johnson, E. A. Moore, M. Mortimer, F. F. F. Vetel, *J. Mater. Chem.* **2000**, *10*, 2131.

[18] É. Tóth, L. Helm, A. E. Merbach in, *The Chemistry of Contrast Agents in Medical Magnetic Resonance Imaging* (Eds.: A. E. Merbach, É. Tóth), Wiley, Chichester, **2001**, Chapter 2, pp. 45–119.

[19] Y.-S. Lin, Y. Hung, J.-K. Su, R. Lee, C. Chang, M.-L. Lin, C.-Y. Mou, *J. Phys. Chem. B.* **2004**, *108*, 15608.

[20] J. Dexpert-Ghys, C. Picard, A. Taurines, *J. Inclusion Phenom. Macrocyclic Chem.* **2001**, *39*, 261.

[21] H. Klein, H. Fuess, *J. Chem. Soc. Faraday Trans.* **1995**, *91*, 1813.

[22] W. D. Basler, *Ber. Bunsenges. Phys. Chem.* **1978**, *82*, 1051.

[23] R. A. Brooks, F. Moiny, P. Gillis, *Magn. Reson. Med.* **2001**, *45*, 1014.

[24] A. C. McLaughlin, J. S. Leigh Jr., *J. Magn. Reson.* **1973**, *9*, 296.

[25] J. S. Leigh Jr., *J. Magn. Reson.* **1971**, *4*, 308.

[26] C. F. Hazlewood, D. C. Chang, B. L. Nichols, D. E. Woessner, *Biophys. J.* **1974**, *14*, 583.

Received: January 13, 2005
Published online: June 1, 2005

